

MODELING FOR DISPERSION AND LOSSES OF MULTILAYER ASYMMETRIC CPW ON ISO/ANISOTROPIC SUBSTRATE

Anand K. Verma, Paramjeet Singh*, and Ritu Bansal

Microwave Research Laboratory, Department of Electronic Science, University of Delhi South Campus, New Delhi 110021, India

Abstract—In this paper, we reformulate the quasi-static spectral domain analysis (SDA) applicable to a lossy anisotropic multilayer asymmetric coplanar waveguide (ACPW). The SDA formulation also incorporates *two-layer model* of a conductor thickness and the *concept of effective permeability* to account for the low frequency dispersion due to the magnetic field penetration in an imperfect conductor. The paper further presents the single layer reduction (SLR) formulation and circuit model to compute frequency dependent line parameters of a lossy anisotropic multilayer ACPW. The accuracy of formulation is comparable to that of the HFSS and CST, without using complex and time consuming full-wave methods. The results of CST for ϵ_{eff} , Z_0 , α_d , α_c of multilayer ACPW, in the frequency range 1 GHz–100 GHz, deviate from results of HFSS up to 0.49%, 1.53%, 2.06% and 10.73% respectively; whereas corresponding deviations of the present SDA and SLR combined formulation are up to 1.38%, 2.09%, 3.57% and 8.87%.

1. INTRODUCTION

The standard and multilayer coplanar waveguide (CPW) have been extensively investigated for their applications in MIC, MMIC and MEMS technology. The CPW structures, available in several formats and their circuit and component applications, are summarized in book form [1–3]. Several static and full-wave numerical methods have been used to analyze the CPW structures [3–8]. Using these methods, CPW on the anisotropic substrates have been also studied by several investigators [9–11]; as some practical substrates have anisotropy that must be accounted for in computation of the line parameters. The

Received 11 December 2012, Accepted 6 February 2013, Scheduled 13 February 2013

* Corresponding author: Paramjeet Singh (paramwes@yahoo.co.in).

experimental results of the CPW, in subterahertz frequency range, have also been compared against the results from Sonnet [12]. The *asymmetrical* CPW (ACPW) provides additional degree of freedom in controlling the line parameters — effective relative permittivity and characteristic impedance [5, 10, 11]. The CPW is a less dispersive transmission medium as compared to a microstrip line. The closed-form expressions are reported to compute dispersion in a *symmetrical* CPW with zero conductor thickness and with finite conductor thickness also [13]. The dispersion model is also extended to the ACPW structures [10]. However, these models are not applicable to a multilayer ACPW. Moreover effect of the low frequency dispersion, due to finite strip conductivity [14], on the effective relative permittivity and characteristic impedance has not been incorporated in the closed-form model. The conductor and dielectric losses are computed using the Wheeler's incremental inductance rule and perturbation method [15–20]. The full-wave methods provide results on dispersive, simple and multilayered CPW, including conductor and dielectric losses. However, these methods are time consuming and not CAD oriented. The quasi-static Galerkin's method is capable to provide static characteristic impedance and effective relative permittivity of a multilayer ACPW [3, 21]. The available formulation does not account for the strip conductor thickness. Moreover we need computation of dispersion, dielectric loss and conductor loss of a multilayer ACPW without using the full-wave methods. Such process could be faster and CAD oriented, useful for both the analysis and synthesis of the multilayer ACPW based components and circuits. These expressions could be also useful to analyze propagation of pulses on a multilayer ACPW [13].

The present work, in Section 2, reformulates the Galerkin's method based spectral domain analysis (SDA) for a lossy anisotropic multilayer ACPW with finite strip thickness and finite conductivity. We introduce the concept of the *effective inductance* to account for the effect of the finite strip conductivity on the low frequency dispersion both in the effective relative permittivity and characteristic impedance of an ACPW. The effect of conductor thickness is accounted for by accommodating the *two-layer strip conductor model* that is suggested for a microstrip line [22]. In the Section 3 the single layer reduction (SLR) method [18, 20, 23–25], along with the concept of the *equivalent symmetrical gap — width* that converts the ACPW to an equivalent symmetrical CPW, is used to compute the dispersion, dielectric loss and conductor loss of a multilayer ACPW. Finally a circuit model is used that accurately computes frequency dependent complex propagation parameters and complex characteristic impedance of a

multilayer lossy ACPW. In Section 4, results of the present method are compared against two commercial 3D EM-simulators — Ansoft HFSS and CST Microwave Studio [26, 27]. Results are also compared against available experimental results [6–8, 10, 11, 28]. We have taken results from two 3D commercial EM-simulators; as the accuracy of the present method should be around the deviation in results from these independent full-wave results. In order to ascertain accuracy of the simulators, the results from both simulators are also tested against the available experimental results. The accuracy of the present formulation is in the range provided by the full-wave method and EM-simulators.

2. SDA FORMULATION OF LOSSY ANISOTROPIC MULTILAYER ACPW

This section considers the following items — Section 2.1: Conversion of multilayer anisotropic substrate to isotropic substrate. Section 2.2: Formulation of the SDA with finite conductor thickness. Section 2.3: Consideration of finite conductivity of the strip conductor.

2.1. Conversion of Multilayer Anisotropic Substrate to Isotropic Substrate

Figure 1 shows a four layered shielded asymmetrical coplanar waveguide (ACPW) of finite conductor thickness. It shows widths of ground conductors, G_1 and G_2 , central strip conductor W and the slot widths, S_1 and S_2 . We have considered the finite conductivity

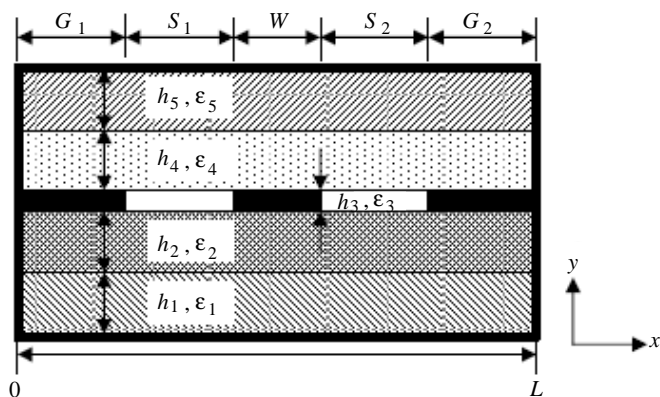


Figure 1. Shielded multilayer coplanar waveguide with finite conductor thickness.

strip conductor as a dielectric layer of relative permittivity ε_3 and thickness h_3 . The lossy anisotropic dielectric layers account for the effect of losses on the line parameters. Practical substrates may have anisotropy, along with losses. The layered ACPW could be reduced to technologically useful shielded, composite and suspended ACPW. The standard symmetrical CPW is obtained for $G_1 = G_2$ and $S_1 = S_2$. The structure is also reduced to a shielded microstrip for $G_1 = G_2 \rightarrow 0$. The bottom of the metallic shield provides a ground plane to the microstrip line.

We compute the complex line capacitance of an anisotropic multilayer ACPW, using the quasi-static spectral domain analysis (SDA) method. It helps us to obtain the static line parameters. Before using the SDA, first we convert the anisotropic dielectric layer to an equivalent isotropic layer. The relative permittivity tensor of a lossy uniaxial anisotropic dielectric is given by

$$\bar{\varepsilon}_{rm}^* = \begin{bmatrix} \varepsilon_{r,xxm}^* & \varepsilon_{r,xym}^* \\ \varepsilon_{r,yxm}^* & \varepsilon_{r,yy}^* \end{bmatrix} \quad (1a)$$

where

$$\begin{aligned} \varepsilon_{r,xxm}^* &= \varepsilon_{r\parallel m}^* \cos^2 \theta + \varepsilon_{r\perp m}^* \sin^2 \theta \\ \varepsilon_{r,yy}^* &= \varepsilon_{r\parallel m}^* \sin^2 \theta + \varepsilon_{r\perp m}^* \cos^2 \theta \\ \varepsilon_{r,xym}^* &= (\varepsilon_{r\parallel m}^* - \varepsilon_{r\perp m}^*) \sin \theta \cos \theta \end{aligned} \quad (1b)$$

where $m = 1, 2, 4, 5$ are dielectric layers, and θ is the angle between the crystal axis and physical axis of the structure. Each layer of the anisotropic substrate is replaced by an equivalent isotropic dielectric substrate with equivalent relative permittivity and equivalent height given by the following equations [29]:

$$\varepsilon_{reqm}^* = \sqrt{\varepsilon_{r,xxm}^* \varepsilon_{r,yy}^* - (\varepsilon_{r,xym}^*)^2} \quad (2a)$$

$$h_{eqm} = h_m \operatorname{Re} \left(\sqrt{\frac{\varepsilon_{r,xxm}^*}{\varepsilon_{r,yy}^*} - \left(\frac{\varepsilon_{r,xym}^*}{\varepsilon_{r,yy}^*} \right)^2} \right) \quad (2b)$$

$$\tan \delta_m = \frac{\varepsilon_{r,xx}''}{\varepsilon_{r,xx}'} = \frac{\varepsilon_{r,yy}''}{\varepsilon_{r,yy}'} \quad (2c)$$

$$\varepsilon_{r,xxm}^* = \varepsilon_{r,xxm}' - j\varepsilon_{r,xxm}'' \text{ etc.} \quad (2d)$$

where h_m is thickness of the m th anisotropic dielectric layer and h_{eqm} is thickness of the m th equivalent isotropic dielectric layer ($m = 1, 2, \dots$). In our further discussion, with respect to Figure 1, we adopt simpler nomenclature by replacing $\varepsilon_{reqm}^* \rightarrow \varepsilon_m$, $h_{eqm} \rightarrow h_m$.

2.2. Formulation of the SDA with Finite Conductor Thickness

The SDA formulation first converts the two dimensional Laplace’s partial differential equation in the space domain to an ordinary 2nd order differential equation in the Fourier domain. The unknown charge distributions on the strip conductors are expanded in terms of the assumed basis functions and finally the equation is solved with help of Galerkin’s technique [3, 21]. The transverse transmission line (TTL) technique is used to obtain the dyadic Green’s function of the multilayer structure [30]. The Green’s function, showing the potential distribution function, in the discrete Fourier domain, is obtained by solving the following Laplace’s equation:

$$\frac{\partial^2 \tilde{G}(\beta_n)}{\partial y^2} - \beta_n^2 \tilde{G}(\beta_n) = 0 \tag{3a}$$

$$\beta_n = \frac{(2n - 1)\pi}{2L}, \quad n = 1, 2, 3 \dots \tag{3b}$$

where β_n is the discrete Fourier variable. The *two-layer conductor model* [22] is used to account for the finite conductor thickness. The combined charges, on the strip and ground conductors, create potential at any layer of an ACPW. In Fourier domain, this potential is just a multiplication of the dyadic Green’s function and summation of charges on three conductors. The Fourier domain potential at the plane containing strip conductors, in the range $[0, L]$, is also a combination of potentials on the conducting strips $\tilde{V}_c(\beta_n)$ and in the slot regions $\tilde{V}_d(\beta_n)$. Therefore, the potential due to the basis charge density function $\tilde{\rho}_{s1i}(\beta_n)$, $\tilde{\rho}_{s2i}(\beta_n)$ and $\tilde{\rho}_{s3i}(\beta_n)$ is related to the Green’s function as follows:

$$\tilde{G}(\beta_n) \tilde{\rho}_s(\beta_n) = \tilde{V}_c(\beta_n) + \tilde{V}_d(\beta_n) \tag{4}$$

The *two-layer conductor model* considers the finite thickness of the conductor as two conducting surfaces — surface-1 and surface-2, separated by thickness h_3 . The charges reside on both surfaces and in between medium is a dielectric layer with $\epsilon_r = 1$. The above expression is adopted, using the complex dyadic Green’s function, to the two-layer conductor model as follows:

$$\begin{aligned} & \begin{bmatrix} \tilde{G}_{11}(\beta_n) & \tilde{G}_{12}(\beta_n) \\ \tilde{G}_{21}(\beta_n) & \tilde{G}_{22}(\beta_n) \end{bmatrix} \begin{bmatrix} \sum_{i=1}^N a_i^1 \tilde{\rho}_{s1i}(\beta_n)_+ & \sum_{i=1}^N b_i^1 \tilde{\rho}_{s2i}(\beta_n)_+ & \sum_{i=1}^N c_i^1 \tilde{\rho}_{s3i}(\beta_n)_+ \\ \sum_{i=1}^N a_i^2 \tilde{\rho}_{s1i}(\beta_n)_+ & \sum_{i=1}^N b_i^2 \tilde{\rho}_{s2i}(\beta_n)_+ & \sum_{i=1}^N c_i^2 \tilde{\rho}_{s3i}(\beta_n)_+ \end{bmatrix} \\ & = \begin{bmatrix} \tilde{V}_c^1(\beta_n)_+ & \tilde{V}_d^1(\beta_n)_+ \\ \tilde{V}_c^2(\beta_n)_+ & \tilde{V}_d^2(\beta_n)_+ \end{bmatrix} \tag{5} \end{aligned}$$

The charge density basis functions, on both the lower and upper layers, are confined to the strip conductors and are zero outside the strips. The space variable basis functions are taken as $\rho_{s1i}(x)$, $\rho_{s2i}(x)$, $\rho_{s3i}(x)$; with their Fourier transformed basis functions as $\tilde{\rho}_{s1i}(\beta_n)$, $\tilde{\rho}_{s2i}(\beta_n)$, $\tilde{\rho}_{s3i}(\beta_n)$, for the charge density on the central strip W , left ground G_1 and right ground G_2 strip respectively; where $i = 1, 2, 3, \dots, N$ is the number of terms of the basis function. The summation is taken over number of terms of the basis function. The coefficients a_i^p , b_i^p , c_i^p ; $p = 1, 2$ are associated with expansions of charge distribution functions at lower surface ($p = 1$) and at upper surface ($p = 2$) of the strip conductors. We assume the following charge distribution functions both on lower and upper surfaces of the central and ground conductors [3]:

$$\rho_{s1i}(x) = \frac{\cos\left[(i-1)\pi\frac{(x-S_1-G_1)}{W}\right]}{\sqrt{1-\left[\frac{2(x-S_1-G_1)-W}{W}\right]^2}}, \quad (G_1+S_1 \leq x \leq G_1+S_1+W) \quad (6a)$$

$$\rho_{s2i}(x) = \frac{\cos\left[\left(i-\frac{1}{2}\right)\pi\frac{(x-G_1)}{G_1}\right]}{\sqrt{1-\left[\frac{x}{G_1}\right]^2}}, \quad (0 \leq x \leq G_1) \quad (6b)$$

$$\rho_{s3i}(x) = \frac{\cos\left[\left(i-\frac{1}{2}\right)\pi\frac{(x-L+G_2)}{G_2}\right]}{\sqrt{1-\left[\frac{L-x}{G_2}\right]^2}}, \quad (G_1+S_1+W+S_2 \leq x \leq L) \quad (6c)$$

We consider the potential on conducting strips $\tilde{V}_c^p(\beta_n)$ and potential in the slot regions $\tilde{V}_d^p(\beta_n)$, on both the lower and upper layers of the strip conductors separately. Equation (5) is written for each of the lower and upper conducting layers as follows:

$$\begin{aligned} & \tilde{P}_{11}(\beta_n) + \tilde{P}_{12}(\beta_n) + \tilde{P}_{21}(\beta_n) + \tilde{P}_{22}(\beta_n) + \tilde{P}_{31}(\beta_n) + \tilde{P}_{32}(\beta_n) \\ & = \tilde{V}_c^1(\beta_n) + \tilde{V}_d^1(\beta_n) \end{aligned} \quad (7a)$$

$$\begin{aligned} & \tilde{P}_{41}(\beta_n) + \tilde{P}_{42}(\beta_n) + \tilde{P}_{51}(\beta_n) + \tilde{P}_{52}(\beta_n) + \tilde{P}_{61}(\beta_n) + \tilde{P}_{62}(\beta_n) \\ & = \tilde{V}_c^2(\beta_n) + \tilde{V}_d^2(\beta_n) \end{aligned} \quad (7b)$$

The $\tilde{P}(\beta_n)$ parameters, in terms of components of the dyadic Green's function are defined as

$$\tilde{P}_{11}(\beta_n) = \tilde{G}_{11}(\beta_n) \sum_{i=1}^{N_1} a_i^1 \tilde{\rho}_{s1i}(\beta_n) \quad \tilde{P}_{12}(\beta_n) = \tilde{G}_{12}(\beta_n) \sum_{i=1}^{N_1} a_i^2 \tilde{\rho}_{s1i}(\beta_n)$$

$$\begin{aligned}
 \tilde{P}_{21}(\beta_n) &= \tilde{G}_{11}(\beta_n) \sum_{i=1}^{N_1} b_i^1 \tilde{\rho}_{s2i}(\beta_n) & \tilde{P}_{22}(\beta_n) &= \tilde{G}_{12}(\beta_n) \sum_{i=1}^{N_1} b_i^2 \tilde{\rho}_{s2i}(\beta_n) \\
 \tilde{P}_{31}(\beta_n) &= \tilde{G}_{11}(\beta_n) \sum_{i=1}^{N_1} c_i^1 \tilde{\rho}_{s3i}(\beta_n) & \tilde{P}_{32}(\beta_n) &= \tilde{G}_{12}(\beta_n) \sum_{i=1}^{N_1} c_i^2 \tilde{\rho}_{s3i}(\beta_n) \\
 \tilde{P}_{41}(\beta_n) &= \tilde{G}_{21}(\beta_n) \sum_{i=1}^{N_1} a_i^1 \tilde{\rho}_{s1i}(\beta_n) & \tilde{P}_{42}(\beta_n) &= \tilde{G}_{22}(\beta_n) \sum_{i=1}^{N_1} a_i^2 \tilde{\rho}_{s1i}(\beta_n) \\
 \tilde{P}_{51}(\beta_n) &= \tilde{G}_{21}(\beta_n) \sum_{i=1}^{N_1} b_i^1 \tilde{\rho}_{s2i}(\beta_n) & \tilde{P}_{52}(\beta_n) &= \tilde{G}_{22}(\beta_n) \sum_{i=1}^{N_1} b_i^2 \tilde{\rho}_{s2i}(\beta_n) \\
 \tilde{P}_{61}(\beta_n) &= \tilde{G}_{21}(\beta_n) \sum_{i=1}^{N_1} c_i^1 \tilde{\rho}_{s3i}(\beta_n) & \tilde{P}_{62}(\beta_n) &= \tilde{G}_{22}(\beta_n) \sum_{i=1}^{N_1} c_i^2 \tilde{\rho}_{s3i}(\beta_n)
 \end{aligned} \tag{8}$$

The components of the complex dyadic Green’s function are obtained using the transverse transmission line (TTL) technique in Fourier domain [3, 30]. The TTL takes care of the number of dielectric layers. The results are summarized below:

$$\tilde{G}_{11}(\beta_n) = \frac{1}{\beta_n (GF_1 + GF_3)} \tag{9a}$$

$$\tilde{G}_{22}(\beta_n) = \frac{1}{\beta_n (GF_2 + GF_4)} \tag{9b}$$

$$\tilde{G}_{12}(\beta_n) = \tilde{G}_{22}(\beta_n) \left[\frac{\varepsilon_{r3} / \sinh(\beta_n h_3)}{\varepsilon_{r3} \coth(\beta_n h_3) + GF_1} \right] \tag{9c}$$

$$\tilde{G}_{21}(\beta_n) = \tilde{G}_{11}(\beta_n) \left[\frac{\varepsilon_{r3} / \sinh(\beta_n h_3)}{\varepsilon_{r3} \coth(\beta_n h_3) + GF_2} \right] \tag{9d}$$

where parameters $GF_1 - GF_4$ are given below:

$$GF_1 = \varepsilon_{r2} \left[\frac{\varepsilon_{r2} + \varepsilon_{r1} \coth(\beta_n h_1) \coth(\beta_n h_2)}{\varepsilon_{r1} \coth(\beta_n h_1) + \varepsilon_{r2} \coth(\beta_n h_2)} \right] \tag{10a}$$

$$GF_2 = \varepsilon_{r4} \left[\frac{\varepsilon_{r4} + \varepsilon_{r5} \coth(\beta_n h_4) \coth(\beta_n h_5)}{\varepsilon_{r4} \coth(\beta_n h_4) + \varepsilon_{r5} \coth(\beta_n h_5)} \right] \tag{10b}$$

$$GF_3 = \varepsilon_{r3} \left[\frac{\varepsilon_{r3} + \coth(\beta_n h_3) GF_2}{\varepsilon_{r3} \coth(\beta_n h_3) + GF_2} \right] \tag{10c}$$

$$GF_4 = \varepsilon_{r3} \left[\frac{\varepsilon_{r3} + \coth(\beta_n h_3) GF_1}{\varepsilon_{r3} \coth(\beta_n h_3) + GF_1} \right] \tag{10d}$$

In above expressions relative permittivity of each layer is a complex quantity. For anisotropic case, it shows equivalent relative permittivity and h_m shows equivalent substrate thickness given in

Equations (2a)–(2d). The coefficients a_i^p , b_i^p , c_i^p ; $p = 1, 2$ associated with expansions of charge distribution functions used in Equation (8), are determined by taking the inner products with six testing functions. Six basis functions, three for lower conductor surface and three for upper conductor surface, are taken as the testing functions. Resulting six equations are solved with help of Parseval's identity to get the distribution expansion coefficients a_i^1 and a_i^2 on the central strip. We compute the line capacitance of a multilayer ACPW by following expression [21]:

$$\frac{C}{\varepsilon_o} = \sum_{i=1}^N (a_i^1 Q_i + a_i^2 Q_i) \quad (11)$$

The charge Q_i on the central conductor due to the i th basis function is given by

$$Q_i = \int_{G_1+S_1}^{G_1+S_1+W} \frac{\cos \left[(i-1) \pi \frac{(x-S_1-G_1)}{W} \right]}{\sqrt{1 - \left[\frac{2(x-S_1-G_1)-W}{W} \right]^2}} dx \quad (12)$$

Finally the complex effective dielectric constant ($\varepsilon_{\text{reff}}^*$) and complex characteristic impedance (Z_0^*) of a lossy anisotropic multilayer ACPW are obtained as follows:

$$\varepsilon_{\text{reff}}^* = \frac{C_d^*(\varepsilon_r^*)}{C_a(\varepsilon_r = 1)} \quad (13a)$$

$$Z_0^* = \frac{1}{c_o \sqrt{C_d^*(\varepsilon_r^*) C_a(\varepsilon_r = 1)}} \quad (13b)$$

where c_o is velocity of the EM-wave in the free-space. The complex line capacitance $C_d^*(\varepsilon_r^*)$ is on the lossy dielectric layers and $C_a(\varepsilon_r = 1)$ is on the air-substrate. The effect of finite strip conductor thickness on $\varepsilon_{\text{reff}}^*$ and Z_0^* is accounted for in our formulation.

2.3. Consideration of Finite Conductivity of the Strip Conductor

In the above formulation, conductivity of strip conductors is ignored. The magnetic field penetrates the strip conductors with finite conductivity. The penetration of magnetic field inside the strip conductors, at low microwave frequency, creates the *effective relative permeability* $\mu_{\text{reff}}(\delta_s)$ in an ACPW that increases its $\varepsilon_{\text{reff}}^*$ and Z_0^* with decrease in operating frequency [14]. The low frequency dispersion in

an ACPW is dominant at frequency below 1 GHz. The $\mu_{\text{reff}}(\delta_s)$ of an ACPW is associated with the skin-depth and it is computed as follows:

$$\mu_{\text{reff}}(\delta_s) = \frac{C_0(\delta_s = 0, \varepsilon_r = 1)}{C_0(\delta_s, \varepsilon_r = 1)} \quad (14)$$

where $C_0(\delta_s = 0, \varepsilon_r = 1)$ is the line capacitance of ACPW, on the air-substrate, without skin-effect i.e. on the perfect conductor, and $C_0(\delta_s, \varepsilon_r = 1)$ is the line capacitance with the skin-depth (δ_s). The skin-depth penetration reduces width of the central strip conductor to $(W - \delta_s)$, and increases the slot-gap to $S_1 + \delta_s$ and $S_2 + \delta_s$. So the magnetic field penetration decreases the line capacitance. Equation (11) computes the line capacitances under both conditions. At lower frequency, reduction in the line capacitance is more, resulting in $\mu_{\text{reff}}(\delta_s) \gg 1$. On other hand, with increase in frequency, the line capacitance increases towards no field penetration case, resulting in $\mu_{\text{reff}}(\delta_s) \rightarrow 1$. The following expressions, for the quasi-static $\varepsilon_{\text{reff}}^*$ and Z_0^* , account for the lower frequency dispersion in the ACPW. The dispersion at higher frequency for the multilayer ACPW is discussed in the next section.

$$\varepsilon_{\text{reff}}^*(\delta_s) = \frac{C_d^*(\varepsilon_r^*)}{C_a(\varepsilon_r = 1)} \mu_{\text{reff}}(\delta_s) \quad (15a)$$

$$Z_0^*(\delta_s) = \frac{1}{c_0} \sqrt{\frac{\mu_{\text{reff}}(\delta_s)}{C_d^*(\varepsilon_r^*) C_a(\varepsilon_r = 1)}} \quad (15b)$$

3. SINGLE LAYER REDUCTION (SLR) FORMULATION OF SHIELDED MULTILAYER ACPW

In this section we discuss the following items: Section 3.1: SLR formulation to get the equivalent single layer ACPW. Section 3.2: Conversion of asymmetrical CPW to the equivalent symmetrical CPW. Section 3.3: Computation of dispersion. Section 3.4: Computation of losses and Section 3.5: Circuit model of the multilayer ACPW.

3.1. SLR Formulation to Get Equivalent Single Layer ACPW

The single layer reduction (SLR) technique, based on the Wheeler's transformation of the multilayer inhomogeneous medium to the homogeneous medium and back to the single layer substrate, has been successfully used in case of the multilayer microstrip line to compute its dispersion, conductor loss and dielectric loss up to mm-wave [18, 20, 23, 24]. The SLR works effectively for the multiple

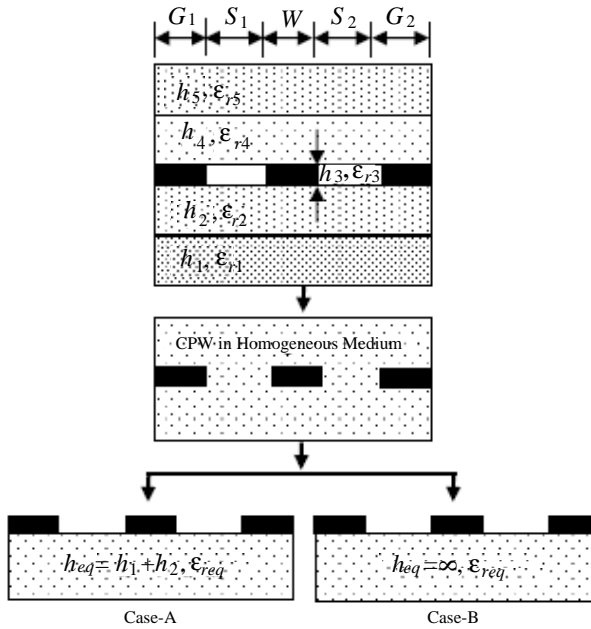


Figure 2. SLR process to get ACPW on equivalent single layer substrate.

dielectric layers between the strip conductor and bottom ground plane. However, it does not work properly for the dielectric superstrate [25]. For the static case, the SLR converts the lossy multilayer ACPW to an equivalent single layer ACPW with equivalent relative permittivity, ϵ_{req} and equivalent loss-tangent, $\tan \delta_{eq}$ in order to compute dispersion and dielectric loss in a multilayer ACPW. In case of anisotropic dielectric layer, first we get the equivalent isotropic layer, as discussed in the previous section, and then apply the SLR process discussed below.

The standard expression to compute dispersion in a symmetrical CPW is applicable to a finite substrate thickness single layer substrate; whereas the standard expression to compute the dielectric loss is applicable to the infinitely thick single layer substrate. Therefore, Figure 2 shows two cases for obtaining the equivalent single layer substrate for a multilayer ACPW. We note that strip dimensions are unchanged in the SLR process. case-A, with finite thickness substrate ($h_{eq} = h_1 + h_2$) is applicable to the dispersion modeling and case-B, with infinite thickness substrate ($h_{eq} \rightarrow \infty$) is applicable to the dielectric loss modeling of a multilayer ACPW. Figure 2 shows that the SLR process works in two steps [23, 24, 31]:

Step-1: This step is called the *Wheeler's transformation*. It is implemented using the static-SDA discussed in previous section. It transforms a lossy multilayer *inhomogeneous* medium ACPW to a lossy *homogeneous* medium with complex relative permittivity ϵ_{reff}^* in which ACPW is embedded.

$$\epsilon_{reff}^* = \frac{C_d^*(\epsilon_r^*)}{C_a(\epsilon_r = 1)} = \epsilon'_{reff} - j\epsilon''_{reff} = \epsilon'_{reff} - j\epsilon'_{reff} \tan \delta_{eff} \quad (16)$$

Step-2: This step is called the *inverse Wheeler's transformation*. It transforms the ACPW located in a lossy *homogeneous* medium to an ACPW on the *equivalent single layer substrate* with equivalent relative permittivity, ϵ'_{req} and equivalent loss-tangent, $\tan \delta_{eq}$.

$$\epsilon'_{req} = \frac{(\epsilon'_{reff} - 1)}{q} + 1 \quad (17a)$$

$$\tan \delta_{eq} = \frac{\epsilon''_{req}}{\epsilon'_{req}} = \frac{\epsilon''_{reff}}{\epsilon'_{reff} + q - 1} \quad (17b)$$

For case-A, we get the ACPW on the single layer substrate with finite equivalent thickness $h_{eq} = h_1 + h_2$, i.e., a sum of substrate thicknesses between the strip conductor and bottom ground conductor. The filling-factor q of the ACPW on single layer substrate, using elliptic function $K(k)$, for this case is [1]

$$q = \frac{1}{2} \frac{K(k'_1) K(k_0)}{K(k_1) K(k'_0)} \quad (18a)$$

$$\text{where } k_0 = \sqrt{\frac{2a(b_1 + b_2)}{(b_1 + a)(b_2 + a)}}, \quad k'_0 = \sqrt{1 - k_0^2} \quad (18b)$$

$$k_1 = \sqrt{\frac{2 \sinh(\pi a/2h_{eq}) [\sinh(\pi b_2/2h_{eq}) + \sinh(\pi b_1/2h_{eq})]}{[\sinh(\pi a/2h_{eq}) + \sinh(\pi b_1/2h_{eq})] [\sinh(\pi a/2h_{eq}) + \sinh(\pi b_2/2h_{eq})]}} \quad (18c)$$

$$k'_1 = \sqrt{1 - k_1^2}$$

The variables a , b_1 and b_2 of the above equations are related to the strip width (W) and two slot-gap widths S_1 and S_2 as $W = 2a$, $b_1 = S_1 + a$, $b_2 = S_2 + a$. For case-B of Figure 2, i.e., the ACPW on the single layer substrate with infinitely thick substrate, we use filling-factor $q = 1/2$ [1].

3.2. Conversion of ACPW to equivalent symmetrical CPW

The available dispersion expression is applicable to a *symmetrical* CPW on the single layer finite thickness substrate. Therefore, we have

to convert the ACPW to a symmetrical CPW with slot-gap width S_{eq} in terms of S_1 and S_2 . It is achieved by using the concept of *weighting factors* that redistribute total capacitance of the asymmetrical CPW for the slot-gap S_1 and S_2 . The weighting factors are obtained on the air-substrate ($\varepsilon_{req} = 1$). It is a function of slot-gaps S_1 , S_2 and conductor thickness h_3 [10]. The equivalent symmetrical slot-gap width S_{eq} is

$$S_{eq} = WF_1 \times S_1 + WF_2 \times S_2 \quad (19)$$

where the weighting factors WF_i ($i = 1, 2$) corresponding to slot-gap S_1 and S_2 are

$$WF_1 = \frac{M_1 D_1}{M_1 D_1 + M_2 D_2}, \quad (20a)$$

$$WF_2 = \frac{M_2 D_2}{M_1 D_1 + M_2 D_2} \quad (20b)$$

$$\text{where } M_1 = 0.15A(1 - A) + 0.5, \quad (20c)$$

$$M_2 = -0.15A(1 - A) + 0.5 \quad (20d)$$

$$D_1 = 4\varepsilon_o \frac{K(k_1)}{K(k'_1)} + 2\varepsilon_o \frac{h_3}{S_1}, \quad (20e)$$

$$D_2 = 4\varepsilon_o \frac{K(k_2)}{K(k'_2)} + 2\varepsilon_o \frac{h_3}{S_2} \quad (20f)$$

The aspect-ratio of elliptic functions are

$$k_1 = \frac{W}{W + 2S_1}, \quad k_2 = \frac{W}{W + 2S_2} \quad (21a)$$

The aspect-ratio of slot-gap is:

$$A = \sqrt{\frac{S_1}{S_2}} \quad (21b)$$

3.3. Computation of Dispersion Characteristics

Over the equivalent single layer substrate, with equivalent symmetrical slot-gap (S_{eq}), we use available dispersion expression [13] to compute dispersion in the multilayer ACPW. The modified quasi-static effective relative permittivity, accounting for the low frequency dispersion, is used. It is discussed in Section 2. The skin-depth dependent improved dispersion expression is a more general expression.

$$\begin{aligned} & \varepsilon_{reff}(f, \delta_s) \\ &= \left[\sqrt{\mu_{eff}(\delta_s) \varepsilon_{reff}(f=0)} + \frac{\sqrt{\varepsilon_{req}} - \sqrt{\mu_{eff}(\delta_s) \varepsilon_{reff}(f=0)}}{(1 + aF^{-b})} \right]^2 \end{aligned} \quad (22)$$

where $F = \frac{f}{f_{TE}}$ and $f_{TE} = \frac{c_0}{4h_{eq}\sqrt{\epsilon_{req}-1}}$ is the cutoff frequency of the TE_1 mode, $b = 1.8$ and

$$\log(a) = u \log\left(\frac{W}{S_{eq}}\right) + v \tag{23a}$$

$$u = 0.54 - 0.64q + 0.015q^2, \quad v = 0.43 - 0.86q + 0.540q^2, \tag{23b}$$

$$q = \log\left(\frac{W}{h_{eq}}\right)$$

The effect of the conductor thickness is accounted for, using *two-layer conductor model*, in computation of the static ϵ_{reff} ($f = 0$). The original expression [13] has accuracy within 5%; for the following range of parameters: $0.1 < W/S_{eq} < 5$, $0.1 < W/h < 5$, $1.5 < \epsilon_r < 50$, $0 < f/f_{TE} < 10$. The dispersive characteristic impedance is computed by the following modified expression that accounts for low frequency dispersion through the concept of the effective relative permeability:

$$Z_0(f, \epsilon_{req}, h_{eq}) = Z_0(f=0, \epsilon_{req}=1, h_{eq}) \sqrt{\frac{\mu_{eff}(\delta_s)}{\epsilon_{reff}(f, \mu_{eff}(\delta_s)=1)}} \tag{24}$$

3.4. Computation of Losses

The dielectric loss of a multilayer ACPW is computed, using the case-B of Figure 2. The equivalent infinitely thick substrate, with equivalent permittivity and equivalent loss-tangent, is obtained from Equations (17a) and (17b) to compute the dielectric loss as follows [20, 31]:

$$\alpha_d = \frac{8.686\pi}{\lambda_0} \frac{\epsilon'_{req}}{\sqrt{\epsilon'_{reff}}} \frac{(\epsilon'_{reff} - 1)}{(\epsilon'_{req} - 1)} \tan(\delta_{eq}) \tag{25}$$

The static ϵ'_{reff} for the ACPW is obtained from the SDA formulation. The Wheeler's incremental inductance method [18] is used to compute the conductor loss of a multilayer ACPW. It involves computation of characteristic impedance with skin-effect and without skin-effect.

$$\alpha_c = \frac{\pi}{\lambda_0} \sqrt{\epsilon'_{reff}} \frac{\Delta Z}{Z(\epsilon_{r1} = \epsilon_{r1} = \dots = 1, h, W, \delta_s, h_3)} \tag{26a}$$

$$\Delta Z = Z(\epsilon_{r1} = \epsilon_{r2} = \dots = 1, W - \delta_s, S_1 + \delta_s, S_2 + \delta_s, h_3 - \delta_s) - Z(\epsilon_{r1} = \epsilon_{r2} = \dots = 1, W, S_1, S_2, h_3) \tag{26b}$$

where δ_s is the skin-depth of the strip conductor.

3.5. Circuit Model of Multilayer ACPW

We have computed above each of line parameters of a multilayer lossy anisotropic substrate ACPW individually using the SLR. The characteristic impedance of a lossy line is a complex quantity. It is obtained by adopting the standard transmission line circuit model to the ACPW. In this process, computation of other line parameters also improves due to mutual interaction of primary line constants of a multilayer ACPW, i.e., resistance (R), conductance (G), capacitance (C) and inductance (L) *p.u.l.* in the circuit model. These frequency dependent line parameters are computed as follows:

$$R(f) = 2Z_0(f)\alpha_c(f) \quad (27a)$$

$$G(f) = \frac{2\alpha_d(f)}{Z_0(f)} \quad (27b)$$

$$C(f) = \frac{\sqrt{\varepsilon'_{reff}(f)}}{c_0 Z_0(f)} \quad (27c)$$

$$L(f) = \frac{Z_0(f)\sqrt{\varepsilon'_{reff}(f)}}{c_0} \quad (27d)$$

The complex characteristic impedance (Z_0^*) and complex propagation constant (γ^*) of the multilayer ACPW are given by

$$Z_0^*(f) = \sqrt{\frac{R(f) + j\omega L(f)}{G(f) + j\omega C(f)}} \quad (28a)$$

$$\gamma^*(f) = \sqrt{(R(f) + j\omega L(f))(G(f) + j\omega C(f))} \quad (28b)$$

The above expressions provide frequency dependent real and imaginary parts of the complex characteristic impedance, more accurate results of the dielectric and conductor losses and frequency dependent effective relative permittivity, $\varepsilon_{reff}(f) = (\beta/\beta_0)^2$. We validate below the SLR based line parameters and also line parameters obtained from the circuit model against the results obtained from the full-wave analysis, experiments and commercial EM-simulators.

4. NUMERICAL RESULTS AND DISCUSSION

The standard, i.e., the symmetric CPW is a special case of the ACPW. Similarly isotropic substrate is a special case of the anisotropic substrate. This section covers validation in three steps: i. Comparison of the present models against the full-wave and experimental results [6, 7, 8, 12]. ii. Comparison of results for the line

parameters of isotropic substrate ACPW against two EM-simulators and iii. Comparison of results for the line parameters of anisotropic substrate ACPW against two EM-simulators.

4.1. Comparison of Results of CPW and ACPW against Full-wave and Experimental Results

We have compared the effective relative permittivity and characteristic impedance of an ACPW structure, in frequency range 1 GHz–30 GHz, on an anisotropic sapphire substrate with $\epsilon_{r\perp} = 11.6$, $\epsilon_{r\parallel} = 9.4$, $h = 1.0$ mm, $W = 0.5$ mm, $S_1 = 1.0$ mm and $S_2 = 2.0$ mm. Two cases of conductor thickness are considered $h_3 = 0, 70 \mu\text{m}$. Figure 3

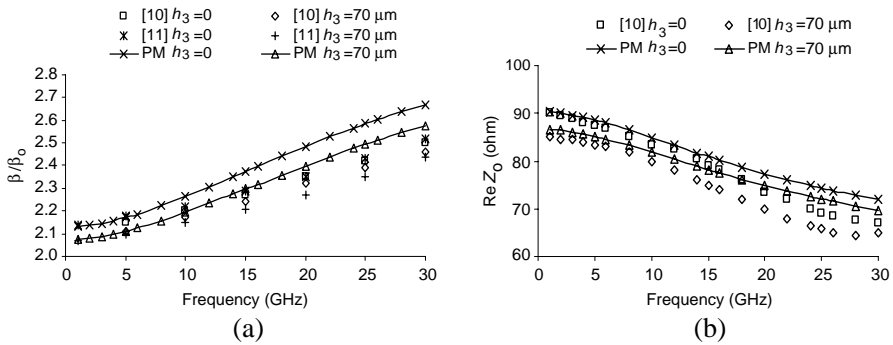


Figure 3. Comparison of $\epsilon_{re\text{ff}}(f)$ and $Z_0(f)$ computed by present method (PM) against full-wave results for the ACPW on anisotropic substrate. (a) Normalizes phase constant. (b) Real characteristic impedance.

Table 1. Comparison of computation of Z_0 against the experimental results.

ACPW No.	Dimensions (μm)			Measured	Calculated		
	W	S_1	S_2	Hanna [6]	Hanna [6]	Karpuz [7]	Present method
1	747	123	1060	51.5	51.78	51.77	52.49
2	737	257	991	57.5	59.88	59.88	60.25
3	735	356	843	61.1	62.96	62.96	62.93
4	1250	196	1756	52.0	53.53	53.51	55.53
5	1248	406	1548	62.4	62.38	62.37	63.68
6	1244	575	1386	66.3	67.17	67.16	67.70

compares the present method (PM) against the results of full-wave methods [11]. The maximum deviation in results is within 3.5% for the characteristic impedance and it is 6.3% for the effective relative permittivity. However it is less than the deviation between two existing methods [10, 11]. Table 1 compares the computation of characteristic impedance as computed by the present method, and also by other methods [6, 7], against the experimental results obtained by the time-domain reflectometer with a 35-ps rise-time pulse, which corresponds to a frequency range from dc to 9.85 GHz. Six ACPW lines are considered on an alumina substrate with $\epsilon_r = 9.9$, $h = 0.635$ mm and gold strip thickness 4.0 μm . The maximum deviation is about 2.0%.

4.2. Comparison of Results of Isotropic Substrate ACPW against EM-simulators

The accuracy of the present models — SDA based SLR and circuit model (CM), for the symmetric CPW on the isotropic substrate, standard single layer and composite layer, has been tested in the frequency range 1 GHz–100 GHz, against two EM-simulators — HFSS [26] and CST [27]. The HFSS is based the finite element method (FEM); while the CST is based on the finite integration technique (FIT) based on FDTD. The strength and weakness of both methods are compared in the literature [32]. The Simulator’s accuracy depends on the implementation of the numerical method, excitation of the port and also on the de-embedding process. Most of these are not controlled by a user. So we have tested accuracy of both the simulators for the symmetrical CPW against the experimental results [28, 33] on single layer GaAs substrate and three layered MCM-D at 20 GHz. For the GaAs case average deviation in results on Z_0 are 1.92%, 0.61% and 1.82% for the HFSS, CST and the present method respectively. For the $\epsilon_{\text{reff}}(f)$ these deviations are 1.72%, 0.99% and 0.76%. In case of the MCM-D, average deviations in results the HFSS, CST and the present method on Z_0 are 2.07%, 2.91%, and 1.0% and for $\epsilon_{\text{reff}}(f)$ these are 5.68%, 3.39% and 2.29%. In case of the loss computation between 1 GHz–40 GHz average deviations, against the experimental results [33], in the results of HFSS, CST and present method are 23.6%, 32.7% and 19.6%. All three methods have different models for the conductor loss computation giving different accuracy. Thus the results of the simulators and present models are likely to same order of relative deviation among themselves.

We compare results of the CPW/ACPW obtained from the CST and the present method against the results of HFSS. For the single layer we have taken gallium arsenide (GaAs) substrate $\epsilon_{r1} = 1.0$, $h_1 \rightarrow \infty$, $\tan \delta_1 = 0$, $\epsilon_{r2} = 12.9$, $h_2 = 380$ μm , $\tan \delta_2 = 0.0003$,

$\epsilon_{r3} = 1.0$, $\epsilon_{r5} = 1.0$, $h_4 = 0$, $h_5 \rightarrow \infty$ and $W = 24 \mu\text{m}$, $S_1 = 18 \mu\text{m}$, $S_2 = 18 \mu\text{m}$. For the composite substrate we have considered GaAs on the alumina substrate, $\epsilon_{r1} = 9.4$, $\tan \delta_1 = 0.001$, $\epsilon_{r2} = 12.9$, $h_2 = 254 \mu\text{m}$, $\tan \delta_2 = 0.0003$, $h_4 = 0$. The strip conductors have $\sigma = 4.1 \times 10^7 \text{ S/m}$ and thickness is $h_3 = 3 \mu\text{m}$. The shield height is $h_5 = 10H$ ($H = h_1 + h_2$). In case of ACPW, we have taken $W = 24 \mu\text{m}$, $S_1 = 12 \mu\text{m}$, $S_2 = 24 \mu\text{m}$; while maintaining same data on the substrate.

Table 2 shows the % deviation in the present models for computation of the $\epsilon_{reff}(f)$, $Z_0(f)$, dielectric, conductor losses and total losses. The circuit model computes the total loss; it does not compute dielectric and conductor loss separately. Therefore α_c and α_d for the circuit model (CM) are not shown in Table 2 and also in Table 3. Almost similar % deviations are obtained for both for the present model and CST. The circuit model shows more accurate results for the total loss. Figure 4 compares the performances of the present model and

Table 2. % Average deviation in symmetric and asymmetric CPW on isotropic substrate against results of HFSS ($h_3 = 3 \mu\text{m}$, $\sigma = 4.1 \times 10^7 \text{ S/m}$, 1 GHz–100 GHz).

	ϵ_{eff}	Z_0	α_d	α_c	α_T
Symmetrical standard CPW $W = 24 \mu\text{m}$, $S_1 = 18 \mu\text{m}$, $S_2 = 18 \mu\text{m}$					
CST	0.35	1.07	0.25	10.11	10.0
SLR	0.90	1.29	0.96	8.83	8.77
CM	0.85	1.28	#	#	8.73
Symmetrical composite Substrate CPW					
CST	0.81	1.47	0.53	9.91	9.19
SLR	1.04	0.90	1.01	9.74	9.74
CM	0.98	0.88	#	#	9.71
Asymmetrical standard CPW $W = 24 \mu\text{m}$, $S_1 = 12 \mu\text{m}$, $S_2 = 24 \mu\text{m}$					
CST	0.91	1.56	0.63	11.65	11.48
SLR	0.99	1.75	1.18	8.91	8.86
CM	0.93	1.72	#	#	8.82
Asymmetrical composite Substrate CPW					
CST	0.49	1.53	2.06	10.73	10.63
SLR	1.43	2.11	3.57	8.87	8.76
CM	1.38	2.09	#	#	8.81

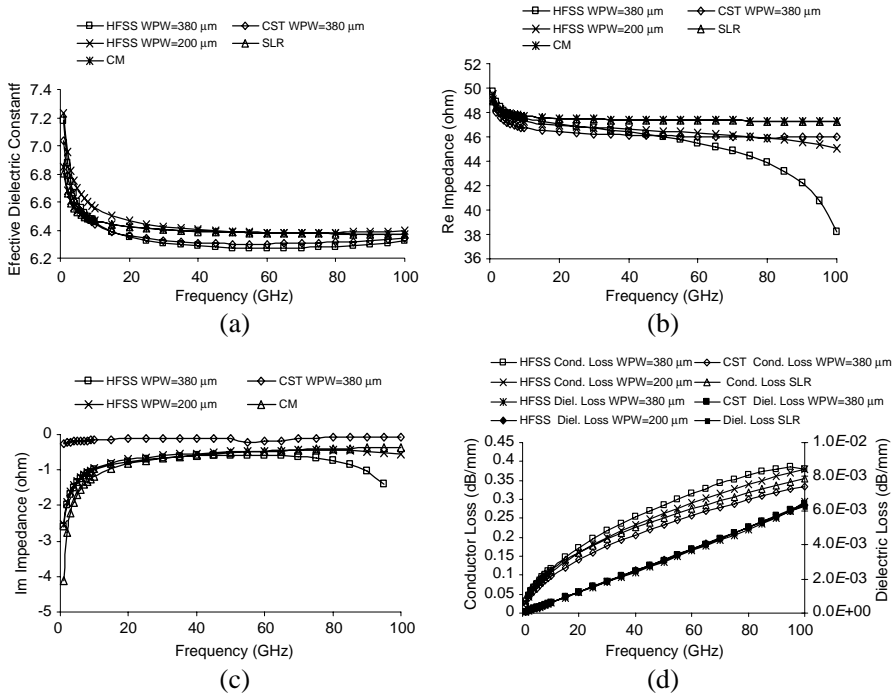


Figure 4. Frequency dependent line parameters of a shielded composite ACPW as obtained using HFSS, CST, SLR, and Circuit Model (CM). (a) Effective dielectric constant. (b) Real characteristic impedance. (c) Imaginary characteristic impedance. (d) Conductor and Dielectric loss.

results of both EM-simulators for the shielded ACPW on the composite substrate over frequency range 1 GHz–100 GHz. Figures 4(a) and 4(b) show that results of $\epsilon_{reff}(f)$ and real $Z_0(f)$, as computed by the present model, are a little above the results of two EM-simulators. The present models follow the results of CST. For these two parameters the SLR shows average deviations 1.43% and 2.11%. We note a marginal improvement in results with the circuit model. The SLR does not compute imaginary part of $Z_0(f)$. It is obtained with help of the circuit model only. In case of the $\text{Im } Z_0(f)$, shown in Figure 4(c), CST does not show low frequency dispersion that is shown by both the present model and HFSS. Figure 4(d) shows that the dielectric losses computed by all models are closer to each other, variation within 3.57%. In case of the conductor loss variation is more between two simulators (10.73%); whereas the present model has less variation (8.87%).

Figure 4(b) shows that the nature of variation for the real $Z_0(f)$, above 60 GHz, provided by HFSS deviates from that of the CST. The

size of the *wave-port* excitation is kept same as that of the cross-section of the CPW structure following the practice suggested in literature [32]. The HFSS has shown presence of a higher order mode at about 40 GHz. This causes decrease in Z_0 and also increase in the conductor loss α_c shown in Figure 4(d). We have reduced width of the wave-port to $200\ \mu\text{m}$ to move the cut-off frequency of the higher order at about 50 GHz. Figure 4(b) shows the flatter behavior of Z_0 up to 100 GHz and it comes closer to the results of CST. Similarly Figure 4(d) shows decrease in α_c and it comes closer to the results of CST, i.e., the deviation between results from both Simulators comes down from 16.98% to 10.73%. The deviation of the present model also reduces from 10.28% to 8.87%. We have noted that results of $\epsilon_{\text{reff}}(f)$ and α_d , obtained from HFSS, are not significantly influenced by reducing the wave-port size.

The higher order mode is not generated from CST simulation; as there is no spike in the frequency domain simulation [27]. Therefore,

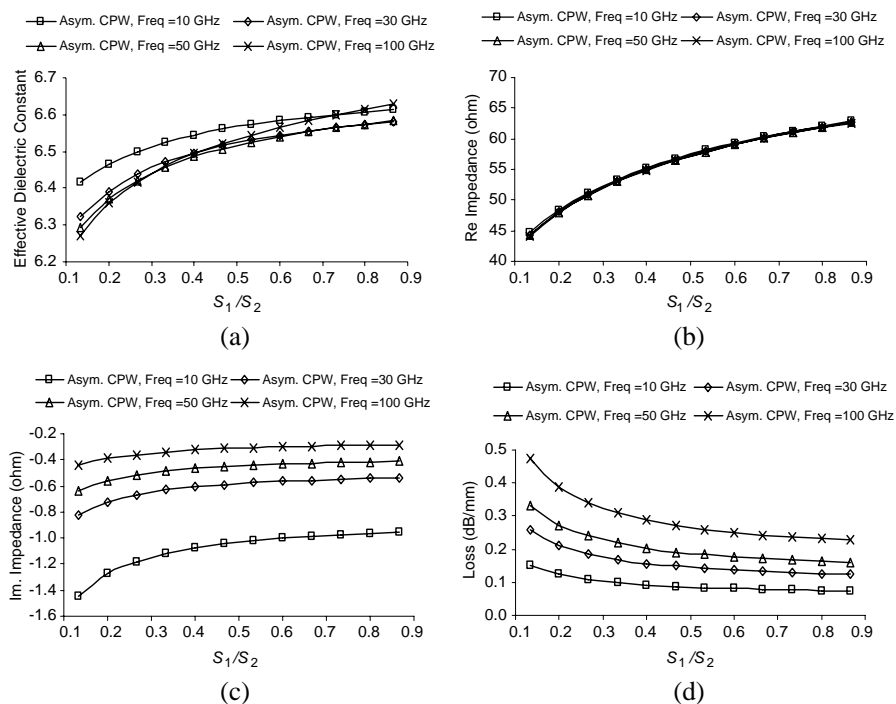


Figure 5. Variation of line parameters of a shielded composite ACPW with respect to asymmetry ratio — S_1/S_2 using circuit model. (a) Effective dielectric constant. (b) Real characteristic impedance. (c) Imaginary characteristic impedance. (d) Total loss.

the results of CST are not significantly influenced by the reduced wave-port size. At this stage we also note that although both the HFSS and CST use the wave-port type excitation; however the HFSS uses 2D simulation to generate the wave-port field and the CST uses 3D simulation of the wave-port field. This difference may have impact on their relative computational accuracy also. The mode generated in the HFSS could be artificial also.

Figures 5(a)–5(d) show variation in line parameters and total loss of the ACPW with respect to the *asymmetry ratio* — S_1/S_2 . The asymmetry controls the real characteristic impedance significantly, from 44Ω to 63Ω with respect to the symmetrical line. This control is almost identical up to 100 GHz. However the $\text{Im } Z_0(f)$ is highly dispersive, but it has small variation with respect to S_1/S_2 . The variation in effective dielectric constant is small with respect to the

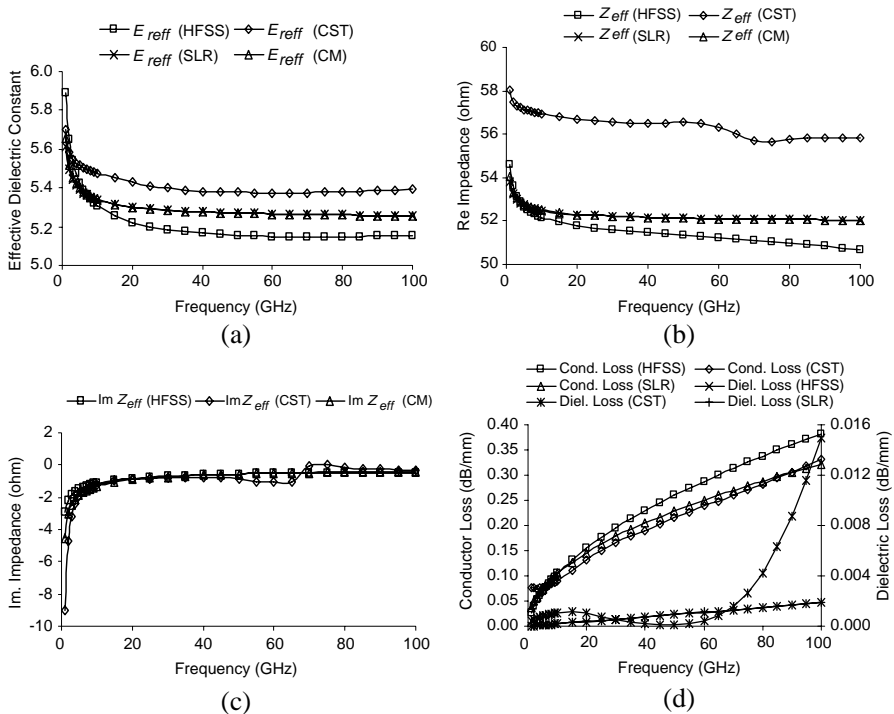


Figure 6. Frequency dependent line parameters of a shielded composite ACPW as obtained using HFSS, CST, SLR and Circuit Model (CM) on anisotropic substrate. (a) Effective dielectric constant. (b) Real characteristic impedance. (c) Imaginary characteristic impedance. (d) Conductor and dielectric loss.

asymmetry ratio — S_1/S_2 and it is larger at higher frequency. The variation in total loss with respect to S_1/S_2 is small. However, it is frequency dependent.

4.3. Comparison of Results of Anisotropic Substrate ACPW against EM-simulators

In Figure 6, we consider the case of a shielded ACPW on the anisotropic composite substrate. The physical ACPW parameters for the composite substrate with respect Figure 1, are $\epsilon_{r1\parallel} = 3.4$, $\epsilon_{r1\perp} = 5.12$, $\epsilon_{r2\parallel} = 11.6$, $\epsilon_{r2\perp} = 9.4$, $\epsilon_{r3} = 1$, $\epsilon_{r5} = 1$, $\tan \delta_{1\parallel,\perp} = 0.0001$, $\tan \delta_{2\parallel,\perp} = 0.0001$, $h_1 = 127 \mu\text{m}$, $h_2 = 254 \mu\text{m}$, $h_3 = 3 \mu\text{m}$, $h_4 = 0$, $h_5 = 10H$, $H = h_1 + h_2$, $W = 24 \mu\text{m}$, $S_1 = 12 \mu\text{m}$, $S_2 = 24 \mu\text{m}$, $\sigma = 4.1 \times 10^7 \text{ S/m}$. The parameters are examined over frequency range 1 GHz–100 GHz. Figures 6(a)–6(d) show results on frequency dependent $\epsilon_{re\text{ff}}(f)$, real and imaginary parts of $Z_0(f)$, and

Table 3. % Average deviation in symmetric and asymmetric CPW on anisotropic substrate against results of HFSS ($h_3 = 3 \mu\text{m}$, $\sigma = 4.1 \times 10^7 \text{ S/m}$, 1 GHz–100 GHz).

	ϵ_{eff}	Z_0	α_d	α_c	α_T
Symmetrical standard CPW					
$W = 24 \mu\text{m}$, $S_1 = 18 \mu\text{m}$, $S_2 = 18 \mu\text{m}$					
CST	2.72	0.80	1058	25.26	25.55
SLR	1.23	1.10	1.00	10.78	10.74
CM	1.18	1.10	#	#	10.71
Symmetrical composite Substrate CPW					
CST	2.13	8.53	357.4	25.17	26.02
SLR	1.06	0.79	1.13	9.67	9.91
CM	1.00	0.78	#	#	9.87
Asymmetrical standard CPW					
$W = 24 \mu\text{m}$, $S_1 = 12 \mu\text{m}$, $S_2 = 24 \mu\text{m}$					
CST	3.73	1.08	452.4	21.76	22.16
SLR	1.66	1.29	1.80	9.75	9.73
CM	1.63	1.26	#	#	9.68
Asymmetrical composite Substrate CPW					
CST	3.53	9.19	457.9	24.52	24.18
SLR	1.75	1.26	1.15	11.43	10.98
CM	1.71	1.25	#	#	10.94

losses as obtained from HFSS, CST, and present model (SLR). The present model and simulators both show low frequency dispersion with high value of $\varepsilon_{reff}(f)$ that comes down with increase in frequency. Usually the results of present model are in between the results of two simulators. For the real $Z_0(f)$, results of the CST are very high; whereas as results of the HFSS and present model are close to each other. For the $\text{Im} Z_0(f)$, all results are close to each other. In case of the dielectric loss, again CST results show a large increase above 70 GHz; whereas the results of HFSS and present model are close to each other. For the conductor loss also the results of present models and CST are close to each other; whereas in this case the results of HFSS are high. It is due the wave-port size as discussed above. The comparison of the results of CST and present model for the symmetrical CPW and ACPW on anisotropic substrate, both single layer (standard) and composite substrate, are summarized in Table 3. In all cases, deviations in results of the present model, against the results of HFSS, are less as compared to the deviation in the results of CST against HFSS.

5. CONCLUSION

In this paper, computationally efficient and analytically simpler, as compared to full-wave methods, quasi-static SDA, applicable to a lossy multilayer anisotropic substrate ACPW, is presented. In the frequency range 1 GHz–100 GHz the CST simulation takes about 9 min; the HFSS takes 5 min; whereas the present method takes less than 2 min for one complete set of results. The present method can be useful for developing the standalone program for the CPW/ACPW structures that can easily accommodate several kinds of physical parameters. The present Galerkin based SDA formulation incorporates the two-layer model of conductor thickness and concept of effective permeability due to magnetic field penetration in the imperfect conductor. This formulation accounts for the effect of conductor thickness and low frequency dispersion on computation of quasi-static effective relative permittivity and characteristic impedance. We have also presented the SLR formulation and circuit model to compute frequency dependent line parameters of a lossy multilayer ACPW. The accuracy of the SDA and SLR combined model is comparable to the accuracy of HFSS and CST, without using the complex and time consuming full-wave methods. The present formulation can be incorporated in the CAD of ACPW based circuits and devices.

ACKNOWLEDGMENT

Authors Acknowledge their gratitude to reviewers for their suggestion to improve the manuscript.

REFERENCES

1. Simon, R. N., *Coplanar Waveguide Circuits Components and Systems*, John Wiley & Sons, New York, 2001.
2. Wolff, I., *Coplanar Microwave Integrated Circuits*, John Wiley & Sons, New York, 2006.
3. Nguyen, C., *Analysis Methods for RF, Microwave, and Millimeter-wave Planar Transmission Line Structures*, John Wiley & Sons, Inc., 2000.
4. Bedair, S. S. and I. Wolff, "Fast accurate and simple approximate analytic formulas for calculating the parameters of supported coplanar waveguides for (M)MIC's," *IEEE Transactions on Microwave Theory and Techniques*, Vol. 40, No. 1, 41–48, Jan. 1992.
5. Gevorgian, S. S., T. Martinsson, P. L. J. Linner, and E. L. Kolberg, "CAD models for multilayered substrate interdigital capacitors," *IEEE Transactions on Microwave Theory and Techniques*, Vol. 44, No. 6, 896–904, Jun. 1996.
6. Hanna, V. F. and D. Thebault, "Theoretical and experimental investigation of asymmetric coplanar waveguides," *IEEE MTT-S Digest*, 469–471, 1984.
7. Karpuz, C., A. Gorur, H. Gorur, and M. Alkan, "Fast and simple analytical expressions for quasistatic parameters of asymmetric coplanar lines," *Microwave and Optical Technology Letters*, Vol. 9, 334–336, Aug. 1995.
8. Chen, P., X. M. Li, S. J. Fang, and S. Q. Fu, "Calculation and analysis of ACPW and UWB ACPW-slotline transition," *International Conference on Signal Processing Systems (ICSPS)*, 644–646, 2010.
9. Kitazawa, T., "Metallization thickness effect of striplines with anisotropic media: Quasi-static and hybrid-mode analysis," *IEEE Transactions on Microwave Theory and Techniques*, Vol. 37, No. 4, 769–775, Apr. 1989.
10. Chang, J. J., "Dispersion characteristics of asymmetrical coplanar waveguide with anisotropic substrate," *International Journal of Microwave and Millimeter-Wave Computer-Aided Engineering*, Vol. 6, No. 3, 166–173, 1996.

11. Kitazawa, T. and T. Itoh, "Asymmetrical coplanar waveguide with finite metallization thickness containing anisotropic media," *IEEE Transactions on Microwave Theory and Techniques*, Vol. 39, No. 8, 1426–1433, Aug. 1991.
12. Zhang, J. and T. Y. Hsiang, "Dispersion characteristics of coplanar waveguides at subterahertz frequencies," *Progress In Electromagnetics Research Symposium*, 232–235, Cambridge, USA, Mar. 26–29, 2006.
13. Hasnain, G., A. Dienes, and J. R. Whinnery, "Dispersion of picosecond pulses in coplanar transmission lines," *IEEE Transactions on Microwave Theory and Techniques*, Vol. 34, No. 6, 738–741, Jun. 1986.
14. Rossi, T. and M. Farina, *Advanced Electromagnetic Analysis of Passive and Active Planar Structures*, 95–96, IEE Pub., U.K., 1999.
15. Duyar, M., V. Akan, E. Yazgan, and M. Bayrak, "Analytical attenuation calculation of asymmetrical coplanar waveguide with finite extent ground planes for coplanar waveguide mode," *Microwave and Optical Technology Letters*, Vol. 49, No. 9, 2082–2087, Sep. 2007.
16. Ghione, G., "A CAD-oriented analytical model for the losses of general asymmetric coplanar lines in hybrid and monolithic MICs," *IEEE Transactions on Microwave Theory and Techniques*, Vol. 41, No. 9, 1499–1510, Sep. 1993.
17. Holloway, C. L. and E. F. Kuester, "A quasi-closed form expression for the conductor loss of CPW lines with an investigation of edge shape effects," *IEEE Transactions on Microwave Theory Techniques*, Vol. 43, No. 12, 2695–2701, Dec. 1995.
18. Singh, H. and A. K. Verma, "Conductor loss of the coplanar waveguide with conductor backing and top shield," *IEEE Asia Pacific Microwave Conference (APMC)*, Delhi, India, 2004.
19. Majumdar, P. and A. K. Verma, "Accurate CAD model of stopping distance to compute conductor loss of CPW," *International Journal Electron. Commun. (AEU)*, Vol. 64, 1157–1166, 2010.
20. Verma, A. K., Nasimuddin, and H. Singh, "Dielectric loss of multilayer coplanar waveguide using the single layer reduction (SLR) formulation," *IEEE Asia Pacific Microwave Conference (APMC)*, China, Dec. 4–7, 2005.
21. Itoh, T., "Generalized spectral domain method for multiconductor printed lines and its application to tunable suspended mi-

- crostrips,” *IEEE Transactions Microwave Theory and Techniques*, Vol. 26, No. 12, 983–987, Dec. 1978.
22. Tripathi, V. K. and R. T. Kollipara, “Quasi-TEM spectral domain analysis of thick microstrip for microwave and digital integrated circuits,” *Electronics Letters*, Vol. 25, No. 18, 1253–1254, Aug. 1989.
 23. Verma, A. K. and G. H. Sadr, “Unified dispersion model for multilayer microstrip line,” *IEEE Transactions on Microwave Theory and Techniques*, Vol. 40, No. 7, 1587–1591, Jul. 1992.
 24. Verma, A. K. and R. Kumar, “New empirical unified dispersion model for suspended, shielded and composite substrate microstrip line for microwave and mm-wave applications,” *IEEE Transactions on Microwave Theory and Techniques*, Vol. 46, No. 8, 1187–1192, Aug. 1998.
 25. Yun, T. Y. and K. Chang, “Analysis and optimization of a phase shifter controlled by a piezoelectric transducer,” *IEEE Transactions on Microwave Theory and Techniques*, Vol. 50, 105–111, Jan. 2002.
 26. Ansoft HFSS V.11.1, Ansoft Corp.
 27. CST Microwave Studio 2009.
 28. Carchon, G., W. De Raedt, and B. Nauwelaers, “Novel approach for a design oriented measurement based fully scaleable coplanar waveguide transmission line model,” *IEE Proc. Microwaves Antennas Propagation*, Vol. 148, No. 4, 227–232, Aug. 2001.
 29. Hoffman, R. K., *Handbook of Microwave Integrated Circuits*, Artech House, 1987.
 30. Cramapgane, R., M. Ahmadpanah, and J. L. Guiraud, “A simple method for determining the Green’s function for a large class of MIC lines having multilayered dielectric structures,” *IEEE Transactions on Microwave Theory and Techniques*, Vol. 26, No. 2, 82–87, Feb. 1978.
 31. Verma, A. K. and A. Bhupal, “Dielectric loss of multilayer microstrip line,” *Microwave and Optical Technology Letters*, Vol. 17, No. 6, 368–370, Apr. 1998.
 32. Swanson, D. G. and J. R. H. Wolfgang, *Microwave Circuit and Medelling Using Electromagnetic Field Simulation*, Artech House, US, 2003.
 33. Ponchak, G. E., I. K. Itotia, and R. F. Drayton, “Propagation characteristics of finite ground coplanar waveguide on Si substrates with porous Si and polyimide interface layers,” *33rd European Microwave Conf.*, 45–48, Munich, 2003.